# Monolithic Phononic Crystals with a Surface Acoustic Band Gap from Surface Phonon-Polariton Coupling

D. Yudistira,[1] A. Boes,[1,2] B. Djafari-Rouhani,[3] Y. Pennec,[3] L. Y. Yeo,[4] A. Mitchell,[1,2] and J. R. Friend[5,6,*]

[1]School of Electrical and Computer Engineering, RMIT University, VIC 3001 Melbourne, Australia

[2]ARC Centre of Excellence for Ultrahigh Bandwidth Devices for Optical Systems, RMIT University, VIC 3001 Melbourne, Australia

[3]Institut d'Electronique, de Microélectronique et de Nanotechnologie (IEMN), UMR CNRS 8520, Université de Lille 1, 59655 Villeneuve d'Ascq Cedex, France

[4]Micro/Nanophysics Research Laboratory, RMIT University, VIC 3001 Melbourne, Australia

[5]Micro/Nanophysics Research Laboratory and the Micro Nano Research Facility, RMIT University, VIC 3001 Melbourne, Australia

[6]Department of Mechanical and Aerospace Engineering, University of California-San Diego, La Jolla, California 92093, USA

(Received 6 May 2014; published 21 November 2014)

We theoretically and experimentally demonstrate the existence of complete surface acoustic wave band gaps in surface phonon-polariton phononic crystals, in a *completely monolithic* structure formed from a two-dimensional honeycomb array of hexagonal shape domain-inverted inclusions in single crystal piezoelectric *Z*-cut lithium niobate. The band gaps appear at a frequency of about twice the Bragg band gap at the center of the Brillouin zone, formed through phonon-polariton coupling. The structure is mechanically, electromagnetically, and topographically homogeneous, without any physical alteration of the surface, offering an ideal platform for many acoustic wave applications for photonics, phononics, and microfluidics.

DOI: 10.1103/PhysRevLett.113.215503 PACS numbers: 63.20.kk, 63.20.dd, 77.65.-j

Phononic crystals (PCs) are artificial structures typically formed through periodic spatial modulation of the elastic impedance [1]. A complete phononic band gap—where no phonon can propagate, irrespective of direction [2,3], the formation of a band-edge state [4], and negative mass density and modulus [5]—is typical of PCs and demonstrates their ability to manage the propagation of phonons for science and applications, ranging from heat management [6] to compact acoustic Bragg confined waveguides [7] and acoustic metamaterial hyperlenses [8]. While the concept of PCs—especially with regard to the formation of a band gap—has been studied for many years [9–11], the existence of a complete gap in PCs is still not obvious. This is especially true for surface acoustic waves (SAW), which has led to significant interest in PCs [2,12,13], particularly in the context of PCs on piezoelectric substrates [14,15] that serve to generate and detect the SAW using interdigital transducers [16].

Traditionally, a complete SAW phononic band gap requires a large contrast between the host matrix and inserted inclusions [1]. SAW PC structures have typically been constructed with a periodic spatial modulation of elasticity $c(\mathbf{x})$, material density $\rho(\mathbf{x})$ [12,13], and piezoelectricity $e(\mathbf{x})$ [14], where $\mathbf{x} \equiv (x, y)$ is the two-dimensional (2D) spatial coordinate, forming a composite of carefully arranged, periodically distributed inclusions in a matrix, most often an array of either holes or pillars in a piezoelectric matrix [14,17]. SAW band gaps have been formed either through a Bragg-scattering mechanism at the Brillouin zone boundaries or through Mie resonances [1].

Recently, we have shown that an oriented SAW band gap may be formed using one-dimensional (1D) periodic domain inversion [18] through phonon-polariton coupling between the electromagnetic wave and acoustic phonons [19]. The SAW band gap is formed in the structure as a result of the superposition of two counterpropagating surface phonons excited through phonon-polariton coupling at a frequency twice that of the Bragg frequency located in the vicinity of the Γ point in the first irreducible Brillouin zone. The phonon-polariton band gap can be formed by simply reversing the sign of the piezoelectric tensor, leaving the density and the elasticity mechanically, electromagnetically, and topographically homogeneous, in extraordinary contrast to past approaches. The existence of a SAW band gap via the 1D periodic domain inversion suggests complete SAW band gaps may exist in the 2D case in much the same way conventional linear optical gratings have been extended to photonic crystals [20].

While there have been a number of studies on phonon-polariton interactions in similar materials in 1D [21–23] and 2D structures [24–26] in the past, none of these papers pertain to phonon-polariton coupling for complete bulk phononic band gaps and, even more so, for complete SAW band gaps. So, in this Letter, we propose a new way to achieve a complete SAW band gap through phonon-polariton coupling in 2D structures that is formed, rather fascinatingly, without any material contrast required except that in the regular, spatial reversal of the piezoelectric coupling tensor. To our knowledge, this is the first

 

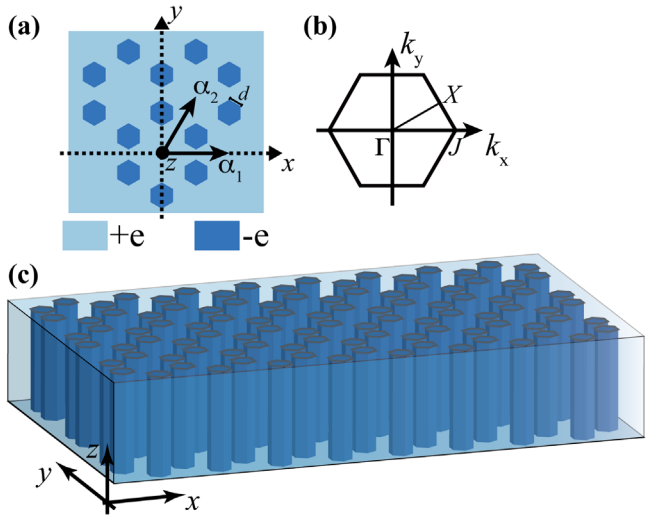


FIG. 1 (color online). Schematic of the proposed surface phonon-polariton PC formed from domain-inverted hexagonal inclusions arranged in a honeycomb lattice. (a) The top view illustrates $\boldsymbol{\alpha}_1 = (a, 0)$ and $\boldsymbol{\alpha}_2 = (a/2, \sqrt{3}a/2)$ as the principal lattice vectors, with lattice constant $a = |\alpha_1| = |\alpha_2|$ and $d$ as the side length of the hexagon. The 2D reciprocal space is presented for (b) the honeycomb lattice and (c) the overall PC structure.

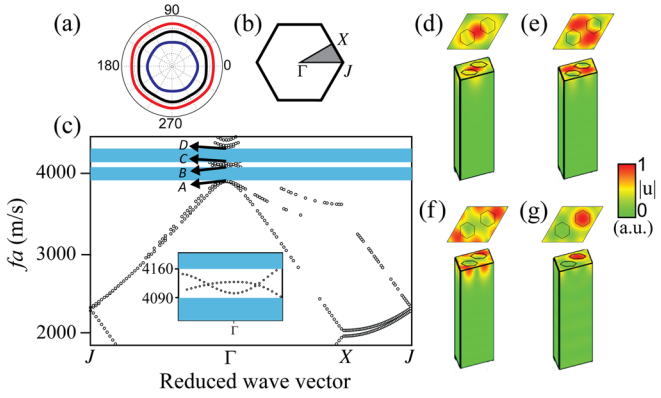


FIG. 2 (color online). (a) Slowness curves of $Z$-cut lithium niobate and (b) the corresponding first irreducible Brillouin zone of the honeycomb lattice, with the triangle $J\Gamma X$ defined by the symmetry of the slowness curve. (c) The SAW band structure calculation of a PC with lattice $d/a = 0.2$; the shaded region indicates the SAW band gaps where the SAW propagation parallel to the $x$-$y$ plane is prohibited. The inset shows the SAW band structure calculated near the $\Gamma$ point at around $fa = 4000$ m/s. (d)–(g) The displacement profiles of the SAW modes calculated at $A$, $B$, $C$, and $D$ in Fig. 2(c).

theoretical prediction and experimental observation of a complete SAW band gap in such PC structures.

Figure 1 illustrates the geometry of the proposed PC, a 2D honeycomb array of hexagonal, domain-inverted inclusions defined along the $x$-$y$ plane of a $Z$-cut lithium niobate crystal. Hexagonal inclusions are straightforward to fabricate in trigonal ($3m$) lithium niobate because the inclusion boundaries fall along symmetry planes in this cut. Other shapes may be possible and beneficial, though this is beyond the scope of this Letter. To investigate the existence of a SAW band gap, we compute the surface acoustic band structure of an infinite periodic honeycomb lattice of the sort indicated in Fig. 1, using finite-element analysis (FEA) [15] by solving the corresponding equations of motion of the structure given by

$$\rho\ddot{u}_j - c^E_{ijkl}\partial_i(\partial_l u_k) - \partial_i[e_{lij}(\mathbf{x})\partial_l\phi] = 0$$
$$\partial_i[e_{ikl}(\mathbf{x})\partial_l u_k] - \epsilon^S_{il}\partial_i(\partial_l\phi) = 0, \qquad (1)$$

where $\mathbf{u}(\mathbf{r}, t)$ is the displacement vector, $\phi(\mathbf{r}, t)$ is the electric potential, $\mathbf{r} \equiv (\mathbf{x}, z) = (x, y, z)$ is the position vector, and $i, j, k, l \in \{1, 2, 3\}$. In Eq. (1), $c^E$ is the stiffness tensor for a constant electric field and $\epsilon^S$ is the permittivity tensor for constant strain, and $e$ is the piezoelectric stress tensor. The mechanical and electromagnetic tensors $c^E$, $\epsilon^S$ are held constant over the entire half-space occupied by the piezoelectric substrate, as is the magnitude of the piezoelectric coupling constant, $e$, but the *signs* of the tensor are dependent upon location $\mathbf{r}$, either positive or negative depending on whether the position is within a domain-inverted inclusion or not.

The $z$ and $x$ axes of the PC are aligned with the crystallographic $Z$ and $X$ axes of the substrate. A hexagonal structure with side length $d = 0.2a$ is considered in this study, arranged to coincide with the crystal's natural preferred domain wall orientation, making an angle of $\pm 60°$ with respect to the $y$ axis, as seen in Fig. 1. Because of the finite system considered in the simulation, spurious and bulk modes satisfying Eq. (1) and the boundary conditions were also found. To identify the surface modes that represent the SAW band structure, we apply mode sorting, considering only modes with 90% of its acoustic energy concentrated within one lattice constant $a$ from the surface. As the lithium niobate crystal is an anisotropic and piezoelectric crystal, the irreducible Brillouin zone depends not only on the symmetry of the PC lattice, as in the case of isotropic materials, but also on the lithium niobate crystal symmetry. The irreducible Brillouin zone can thus be determined from the slowness curve for the slowest bulk wave, a plot of the inverse of the acoustic velocity as a function of the direction of propagation. From the symmetry of the slowness curve of $Z$-cut lithium niobate in Fig. 2(a), the first irreducible Brillouin zone is indicated as the grey triangle $J\Gamma X$ in Fig. 2(b). The band structure calculation was then performed using the reduced wave vector at each edge of the triangle $J\Gamma X$.

Figure 2(c) shows the existence of two complete SAW band gaps around the $\Gamma$ point of the Brillouin zone, as indicated by the shaded region in the figure. The first and second gaps extend from $fa = 3920$ m/s to $fa = 4090$ m/s and $fa = 4160$ m/s to $fa = 4320$ m/s,

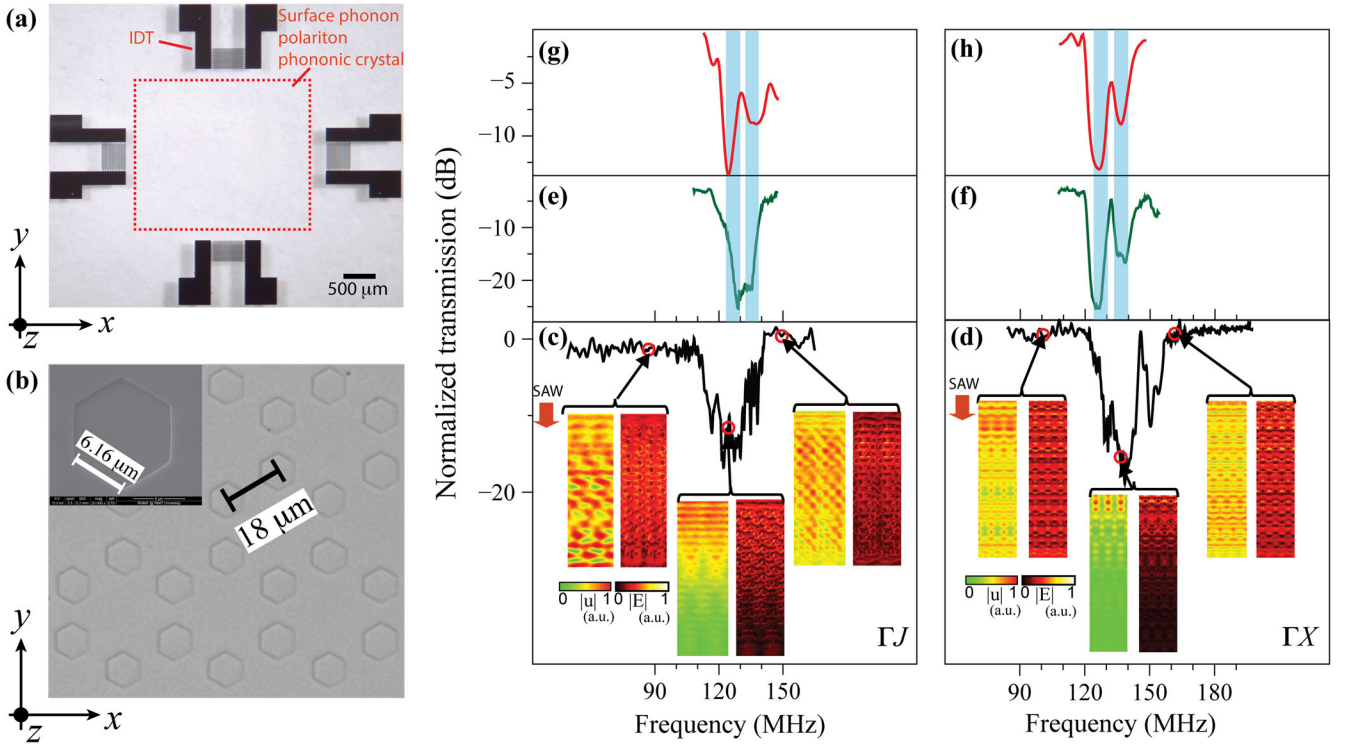


FIG. 3 (color online). (a) SAW delay line structure used to experimentally investigate the SAW band structure of the surface phonon-polariton PC. (b) The honeycomb lattice structure is apparent from an optical micrograph of the back side of the substrate after HF etching, with a scanning electron microscope image inset showing the hexagonal domain-inverted inclusion. (c),(d) The measured and (e), (f) theoretical transmission for surface phonons and (g),(h) for electromagnetic waves for the $\Gamma J$ and $\Gamma X$ orientations, respectively. The shaded region in (e),(f) denotes the expected band gap according to the band structure in Fig. 2(b). The insets in (c),(d) show the top view of the calculated magnitude of the surface phonon displacement and the electric field at frequencies below, within, and above the band gap.

respectively. They are separated by two SAW passbands, as shown in the inset of Fig. 2(c). Their frequencies are approximately twice the Bragg band gap at $fa = 2000$ m/s when it exists. Figures 2(d)–2(g) show the displacement profiles of SAW modes calculated at $A$, $B$, $C$, and $D$ adjacent to the SAW passbands along the $\Gamma$ point in Fig. 2(c), confirming the characteristics of the surface mode as expected.

We fabricated the surface phonon-polariton PC on 500-$\mu$m-thick $Z$-cut lithium niobate using the electric field poling technique [27]. The physical dimensions of the PC are 2.5 mm $\times$ 2.7 mm, as indicated by the dashed region in the optical micrograph of the sample in Fig. 3(a). In contrast with topographic PCs, one can clearly see in Fig. 3(a) that the surface of the PC is uniform, without any alteration of the surface topology.

To reveal and also to analyze the fabricated domain structure of the PC, we etched the back side of the sample with hydrofluoric acid (HF). An optical micrograph of the back side of the PC sample taken after the etching, Fig. 3(b), shows the honeycomb lattice structure and the hexagonal shape of the domain-inverted inclusions, as expected. The distance between the two inclusions is 18 $\mu$m, resulting in a lattice parameter $a = 18\sqrt{3}$ $\mu$m. The measured side length of the hexagon is $d \simeq 6.16$ $\mu$m $\equiv 0.198a$, as shown in the inset of Fig. 3(b). Based on this, the expected frequency gap of the PC is from 126 MHz to 138.5 MHz. The transmission spectra of the phononic crystal along the highest point in the Brillouin zone—namely, $\Gamma J$ and $\Gamma X$, corresponding to the $x$ and $y$ axes, respectively—were subsequently measured [see Fig. 3(a)]. Each SAW delay line used a pair of standard interdigital transducers with 20 finger pairs per transducer for excitation and detection of the SAW. In order to cover the expected band gap, we employed several sets of delay lines with a frequency response from 90 MHz to 190 MHz.

The measured transmission was normalized against the transmission behavior of delay lines without the PC structures. The $\Gamma J$ and $\Gamma X$ direction results are plotted with respect to the frequency shown, respectively, in Figs. 3(c) and 3(d). For comparison, Figs. 3(e) and 3(f) and Figs. 3(g) and 3(h) provide the corresponding numerically derived transmission spectra for surface phonons and electromagnetic waves obtained using FEA of two finite-size (ten-cell) PC structures for the $\Gamma J$ and $\Gamma X$ directions, respectively; the shaded region in these figures indicates the expected band gap, according to the previously calculated band structure. By comparing the experimental and numerical results in Figs. 3(c) and 3(d), one notes a region around

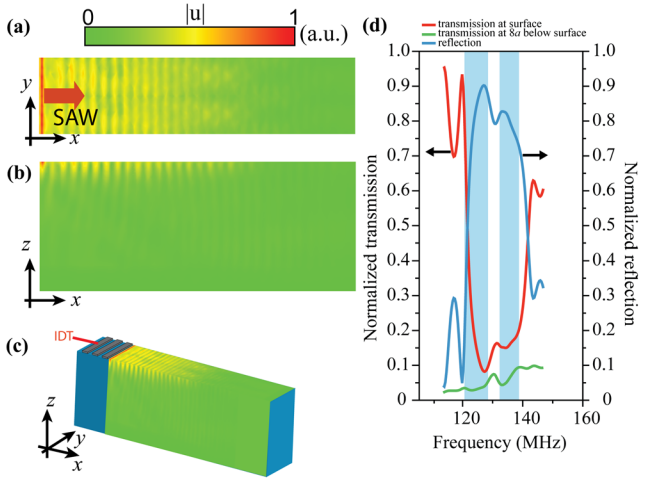


FIG. 4 (color online). Normalized calculated SAW displacement amplitude passing through the PC along the $\Gamma J$ direction at 125 MHz in (a) the $x$-$y$ plane on the top surface and (b) the $x$-$z$ plane, with (c) reference to the full 3D structure. (d) The calculated reflection and the transmission on and 8 wavelengths below the surface, all normalized to the input power.

the expected frequency gap where the SAWs are highly attenuated in both directions.

The results reported in Figs. 3(c)–3(f) provide evidence of the existence of a complete SAW band gap in the surface phonon-polariton PC. A clear discrepancy in the transmission spectra between the calculation and the experiments can be observed, possibly arising either due to differences between the material constants assumed in the calculation and those actually present in the experimental demonstration or due to differences between the inclusion shapes between the fabricated PC and that considered in the calculations [28]. In the $\Gamma J$ direction in Fig. 3(c), one also notices the absence of the passbands that appear in the $\Gamma X$ direction in Fig. 3(d): the SAW band structure calculation predicts its existence, as shown in Fig. 2(c), separating the two band gaps. Based on the symmetry of modes $B$ and $C$ on these bands, it is found that mode $B$ is symmetric with respect to the $y$ axis for the $\Gamma X$ direction and antisymmetric about the $x$ axis for the $\Gamma J$ direction, while mode $C$ is antisymmetric with respect to both $x$ and $y$ axes. Therefore, one may conclude that these passbands are in fact deaf bands [29] for the $\Gamma J$ direction, which then explains the transmission spectra in Figs. 3(c) and 3(d).

Planar views of the calculated spatial distributions of both the surface phonons and the electric field at the frequency below, within, and above the band gap for the $\Gamma X$ and $\Gamma J$ directions are provided in the inset in Figs. 3(c) and 3(d), providing insight into the phonon-polariton coupling present between the surface phonons and the electromagnetic field responsible for the SAW band gap in the PC. One can see a strongly confined electric field at the domain edges inside the PC, revealing the hexagonal domain pattern. This distinction between the acoustic and electric field profiles highlights the phonon-polariton nature of the phononic crystal resonances. At the frequencies within the band gap, both the SAW and the electric field are blocked by the PC, providing experimental support for the prediction that a band gap would be formed by the polariton coupling.

To qualitatively show that the SAW band gap is responsible for the attenuation of the SAW, we plot in Figs. 4(a) and 4(b) the top and side views of the acoustic field amplitude, respectively and Fig. 4(c) providing a 3D isometric view, all calculated at a frequency $f =$ 125 MHz—within the band gap—along the $\Gamma J$ orientation. We also plot in Fig. 4(d) the reflection and the transmission calculated at and 8 wavelengths below the surface—all normalized to the input power. It can be seen that the SAW magnitude is attenuated within the PC due to reflection; coupling into spurious substrate modes by the PC is insignificant, indicating that the radiation loss to other modes is not a factor in the PC's function.

We have predicted and experimentally demonstrated a monolithic surface phonon-polariton PC formed using a periodic arrangement of domain inversions on a lithium niobate crystal. The crystal exhibits a complete SAW band gap, formed through phonon-polariton coupling present at about twice the Bragg band gap at the $\Gamma$ point. The two key advantages offered by this PC are, first, that it is physically formed from a uniform, completely monolithic material and, second, that the structure can be easily formed through electrical poling, a method refined to a fine art over the last decade through advancements in photonics applications. Recent reports [30] have shown that electrical poling can achieve domain sizes as small as 2 $\mu$m, suggesting that it would be possible to construct a PC operating at GHz frequencies. The ability to achieve complete band-gap structures formed from abrupt, precisely defined domain-inverted interfaces should enable extremely accurate phononic crystals with unprecedented surface acoustic wave properties, without the limitations of surface and sidewall roughness or imperfect inclusion geometries typical of past approaches. The monolithic nature of this new PC offers unique opportunities for emerging applications in optomechanical crystals [31] and microfluidics [32,33]. Further, integration of nonlinear parametric optic photonic crystals within this same PC platform offers an entirely new and exciting route to studying resonant phonon-photon interactions.

*jfriend@eng.ucsd.edu

[1] M.-H. Lu, L. Feng, and Y.-F. Chen, Mater. Today **12**, 34 (2009).
[2] B. Djafari-Rouhani, A. A. Maradudin, and R. F. Wallis, Phys. Rev. B **29**, 6454 (1984).
[3] M. S. Kushwaha, P. Halevi, L. Dobrzynski, and B. Djafari-Rouhani, Phys. Rev. Lett. **71**, 2022 (1993).
[4] C. Qiu and Z. Liu, Appl. Phys. Lett. **89**, 063106 (2006).
[5] Y. Ding, Z. Liu, C. Qiu, and J. Shi, Phys. Rev. Lett. **99**, 093904 (2007).

[6] M. Maldovan, Phys. Rev. Lett. **110**, 025902 (2013).
[7] S. Yang, J. H. Page, Z. Liu, M. L. Cowan, C. T. Chan, and P. Sheng, Phys. Rev. Lett. **93**, 024301 (2004).
[8] J. Li, L. Fok, X. Yin, G. Bartal, and X. Zhang, Nat. Mater. **8**, 931 (2009).
[9] R. Martinez-Sala, J. Sancho, J. V. Sanchez, V. Gomez, J. Llinares, and F. Meseguer, Nature (London) **378**, 241 (1995).
[10] W. Cheng, J. Wang, U. Jonas, G. Fytas, and N. Stefanou, Nat. Mater. **5**, 830 (2006).
[11] M. Maldovan, Nature (London) **503**, 209 (2013).
[12] Y. Tanaka and S. Tamura, Phys. Rev. B **58**, 7958 (1998).
[13] T.-T. Wu, L.-C. Wu, and Z.-G. Huang, J. Appl. Phys. **97**, 094916 (2005).
[14] S. Benchabane, A. Khelif, J.-Y. Rauch, L. Robert, and V. Laude, Phys. Rev. E **73**, 065601 (2006).
[15] D. Yudistira, Y. Pennec, B. Djafari-Rouhani, S. Dupont, and V. Laude, Appl. Phys. Lett. **100**, 061912 (2012).
[16] R. M. White and F. W. Voltmer, Appl. Phys. Lett. **7**, 314 (1965).
[17] Y. Achaoui, A. Khelif, S. Benchabane, L. Robert, and V. Laude, Phys. Rev. B **83**, 104201 (2011).
[18] D. Yudistira, A. Boes, D. Janner, V. Pruneri, J. Friend, and A. Mitchell, J. Appl. Phys. **114**, 054904 (2013).
[19] K. Huang, *Dynamical Theory of Crystal Lattices* (Oxford University, New York, 1954).
[20] J. D. Joannopoulos, S. G. Johnson, J. N. Winn, and R. D. Meade, *Photonic Crystals: Molding the Flow of Light*, 2nd ed. (Princeton University, Princeton, NJ, 2008).
[21] Y.-Q. Lu, Y.-Y. Zhu, Y.-F. Chen, S.-N. Zhu, N.-B. Ming, and Y.-J. Feng, Science **284**, 1822 (1999).
[22] C.-P. Huang and Y.-Y. Zhu, Phys. Rev. Lett. **94**, 117401 (2005).
[23] X.-k. Hu, Y. Ming, X.-j. Zhang, Y.-q. Lu, and Y.-y. Zhu, Appl. Phys. Lett. **101**, 151109 (2012).
[24] M.-Y. Yang, L.-C. Wu, and J.-Y. Tseng, Phys. Lett. A **372**, 4730 (2008).
[25] M. Senesi and M. Ruzzene, AIP Adv. **1**, 041504 (2011).
[26] R.-C. Yin, C. He, M.-H. Lu, Y.-Q. Lu, and Y.-F. Chen, J. Appl. Phys. **109**, 064110 (2011).
[27] M. Yamada, N. Nada, M. Saitoh, and K. Watanabe, Appl. Phys. Lett. **62**, 435 (1993).
[28] Y.-Z. Wang, F.-M. Li, W.-H. Huang, and Y.-S. Wang, J. Phys. Condens. Matter **19**, 496204 (2007).
[29] J. V. Sánchez-Pérez, D. Caballero, R. Mártinez-Sala, C. Rubio, J. Sánchez-Dehesa, F. Meseguer, J. Llinares, and F. Gálvez, Phys. Rev. Lett. **80**, 5325 (1998).
[30] A. Busacca, R. Oliveri, A. Cino, S. Riva-Sanseverino, A. Parisi, and G. Assanto, Laser Phys. **17**, 884 (2007).
[31] M. Eichenfield, J. Chan, R. M. Camacho, K. J. Vahala, and O. Painter, Nature (London) **462**, 78 (2009).
[32] J. Friend and L. Y. Yeo, Rev. Mod. Phys. **83**, 647 (2011).
[33] Y. Bourquin, R. Wilson, Y. Zhang, J. Reboud, and J. M. Cooper, Adv. Mater. **23**, 1458 (2011).